Aerospace Science and Technology 117 (2021) 106964

Contents lists available at ScienceDirect

Aerospace Science and Technology

www.elsevier.com/locate/aescte

The formation and development of oblique detonation wave with different chemical reaction models

Hongbo Guo, Xiongbin Jia, Ningbo Zhao *, Shuying Li, Hongtao Zheng, Chengwen Sun, Xiang Chen

College of Power and Energy Engineering, Harbin Engineering University, Harbin, 150001, China

ARTICLE INFO

Article history:
Received 19 October 2020
Received in revised form 24 May 2021
Accepted 12 July 2021
Available online 21 July 2021
Communicated by Yu Lv

Keywords:
Oblique detonation wave
Chemical reaction model
Flow field structure
Radicals formation

ABSTRACT

In this paper, we investigate the formation and development characteristics of oblique detonation wave in stoichiometric hydrogen-oxygen mixtures diluted with argon using Euler equations coupled with the 19-step or 34-step chemical reaction model. The novelty of this work lies in the study of differences in the characteristics of the initiation region and the formation processes of oblique detonation by different chemical kinetic processes. The formation processes of radicals in the induction region and heat release region for the oblique detonation flow field are emphatically analyzed, and the differences in the sensitivity on the key chemical reaction channels to radicals are also discussed. The results show that under the action of 19-step mechanism, the oblique detonation forms relatively early, the wave morphology of the flow field is complex, and the type of the initiation region is abrupt transition. While for the 34-step mechanism, the structure of flow field is simple with smooth transition type. The existence of transverse wave in the mainstream region contributes a lot to the formation of a sonic region and the abrupt transition structure. The chemical kinetic process directly affects the flow field structure of oblique detonation, and H_2O_2 plays an important role on triggering and accelerating the exothermic process. The radicals of H, O and H_2O_2 have different properties in different chemical reaction models.

1. Introduction

In recent years, detonation engines have drawn increasing attention due to their fast heat release and high thermal cycle efficiency in aeronautics and astronautics area [1–5]. Among these detonation engines, the oblique detonation engine (ODE) based on the oblique detonation wave (ODW) is suitable for air-breathing hypersonic aircraft operating at higher flight Mach number than the Scramjet (Supersonic combustion ramjet) [6,7]. Its feasibility and advantage have been demonstrated in some early studies [8–10].

To facilitate the practical application of ODE, the fundamental studies on ODW have been performed to understand the coupling mechanism of oblique shock wave (OSW) and heat release. In earlier investigations, the initiation [11–14] and stabilization [15–19] of ODW are always the key problems. Analytical solutions of the characteristic parameters of the steady ODW such as wave angle and wave morphology are sought by approximating the ODW structure as an oblique shock wave coupled with an instantaneous post-shock heat release [20,21]. Later numerical and experimental investigations have demonstrated that the oblique detonation flow field structure induced by the wedge is more complex. In many cases, an oblique shock wave first forms upon the supersonic inflow mixture interaction with the wedge, and subsequently transits into an oblique detonation wave under the action of combustion induced by OSW [22]. Due to the strong coupling sensitivity between gas dynamics and chemical kinetics [23] as well the inherent unstable nature of detonation wave [24], it remains a technical challenge to establish steady oblique detonations in high-speed combustible mixture for practical propulsion applications. Such success requires fundamental understanding of the formation and development of oblique detonation wave. To this end, the dynamic properties of ODW have attracted much attention in recent years [23].

Using high-resolution numerical simulations, various flow field structures of wedge-induced oblique detonation wave have been revealed [25–35]. Fundamentally, there are two key transition types, namely, the abrupt transition featuring a multi-wave point, and the smooth transition featuring a curved shock [26]. Teng et al. [28] have studied oblique detonation with different chemical kinetic parameters, and obtain the quantitative relationship between the transition structure and oblique shock/detonation wave angle.

* Corresponding author.
E-mail address: zhaoningboheu@126.com (N. Zhao).

https://doi.org/10.1016/j.ast.2021.106964
1270-9638/

It is well established that both the flow conditions and chemical combustion properties determine the possible transition type [28,29,32–35]. The instability of oblique detonation wave is another fundamental characteristic [26,33,36–44]. It is found that the transverse waves or triple structures are more easily formed in the oblique detonation flow field of the combustible mixture with high activation energy [26]. Besides wave morphology, there are also some studies on the surface instability features of ODW [36,43]. The cellular ODW surfaces with different activation energy or wedge angles have been demonstrated by numerical simulations [36,40]. Studies show that the larger the activation energy, the more irregular the detonation cell structure [44]. The oblique detonation wave stems from the OSW-induced combustion process. Hence, the chemical reaction mechanism influences significantly on the formation and development of ODW. For ODW researches, one-step Arrhenius kinetic model is widely used, in which the effects of chemical kinetic parameters are overseen. Two-step induction-reaction global chemistry model has been used to study the influence of induction and reaction parameters on the ODW initiation and surface instability [35,42,45]. It becomes increasing clear that oblique detonation initiation and propagation are mainly affected by the induction time or length scale and chain-branching reactions [46,47]. Yan et al. [48] have analyzed the influences of chemical reaction characteristic parameters in one-step Arrhenius and two-step induction-reaction kinetics on oblique detonation formation and the surface instability. The critical conditions are provided to distinguish the two known ODW transition types. Recent studies [49–52] have proved that the detailed chemical reaction models will considerably influence the detonation characteristics. So, ODW researche based on a detailed chemical model is necessary. Some numerical studies based on detailed chemistry model are also performed, considering issues such as effects of incident Mach number [53], inflow inhomogeneity [30,54] and initiation mechanism [7,13]. Fusina et al. [55] have found that HO_2 radicals play a leading role on the induction region by a detailed chemical reaction model, but the effects of radicals on the internal structures of ODW are still not sufficiently solved.

It is very difficult to form a stationary oblique detonation wave under the condition of supersonic inflow. And the repeatability of experimental researches is poor. Therefore, it is of great significance to carry out numerical simulations on the basic characteristics of oblique detonation, which provides a reliable basis for the design of oblique detonation engine. Hydrogen is a promising fuel for oblique detonation wave engines, which provides higher specific impulse and wider Mach number range than hydrocarbon fuels [56,57]. In this work, the formation and development of ODW in hydrogen-oxygen mixtures diluted with argon are simulated. The 9-species hydrogen-oxygen chemical reaction models, including 19-step and 34-step, are widely used in numerical simulation researches. In order to reveal the influence of chemical processes on the oblique detonation characteristics, the wave system structures and the characteristics of radicals in the oblique detonation flow field with different hydrogen-oxygen chemical reaction models are compared and analyzed.

2. Physical and mathematical models

The schematic of a typical ODW induced by a two-dimensional, semi-infinite wedge is shown in Fig. 1, which also describes the computational setup. The x coordinate is parallel to wedge surface, and Cartesian grid in the rectangular domain enclosed by the dashed line is aligned with the wedge surface. Inflow conditions are interpolated under the assumption of zero first-order derivatives for the left and top boundaries; outflow condition extrapolated from the interior is implemented on the right boundary. Slip reflective boundary condition is used on the wedge surface.

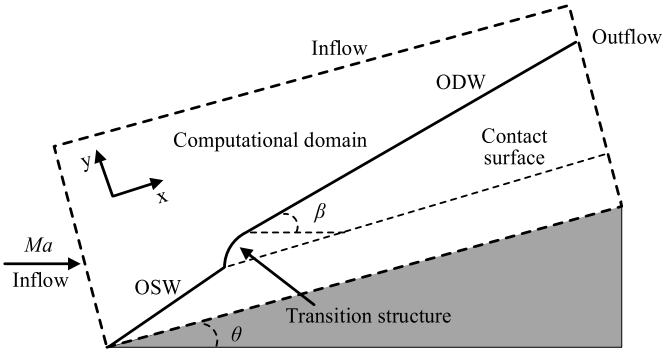

Fig. 1. Schematic of a typical ODW.

Qualitatively, the presence of the wedge in combustible inflow with high Mach number induces an oblique shock wave (OSW). After a chemical reaction induction period, the chemical reaction exothermic process occurs. The oblique detonation wave is formed when the oblique shock wave is coupled with the combustion wave. The inflow velocity for the computational domain is determined by the inflow Mach number Ma and the wedge angle θ. The effects of viscosity and diffusion are ignored, which have insignificant influence on the overall ODW structure [58]. The governing equations for the ODW flow dynamics employed are the 2D Euler equations with chemical kinetics of multi-component system:

$$U_t + [F(U)]_x + [G(U)]_y = S \tag{1}$$

$$\begin{pmatrix} U \\ F(U) \\ G(U) \\ S \end{pmatrix} = \begin{pmatrix} (\rho, & \rho u, & \rho v, & E, & \rho Y_1, & \cdots, & \rho Y_{N-1})^T \\ (\rho u, & \rho u^2 + P, & \rho vu, & (E+P)u, & \rho u Y_1, & \cdots, & \rho u Y_{N-1})^T \\ (\rho v, & \rho uv, & \rho v^2 + P, & (E+P)v, & \rho v Y_1, & \cdots, & \rho v Y_{N-1})^T \\ (0, & 0, & 0, & 0, & \overline{\omega}_1 & \cdots, & \overline{\omega}_{N-1})^T \end{pmatrix} \tag{2}$$

In the above equations, $\overline{\omega}_i$ is the mass production rate of the ith species. Y_i is the mass fraction of ith species. ρ is the total density. P is the pressure. u and v denote the velocity in the direction of x and y. E is the total energy which can be calculated by:

$$E = P + \frac{\rho(u^2 + v^2)}{2} + \rho h \tag{3}$$

where, h is enthalpy per unit mass. Enthalpy and heat capacity for each species are calculated from the data in the JANAF tables [59]. All the gases involved are thermally perfect. As such the equation of state for perfect gas is used.

The above governing equations are coupled with the chemical kinetic law for the reaction rate $\overline{\omega}_i$ that is computed from the Arrhenius equation. The chemical reaction model containing N species and N_R elementary reactions can be uniformly expressed as:

$$\sum_{i=1}^{N} \nu'_{ij} \chi_i \underset{K_{b,j}}{\overset{K_{f,j}}{\rightleftharpoons}} \sum_{j=1}^{N} \nu''_{ij} \chi_i, \quad j = 1, 2, \ldots, N_R \tag{4}$$

where, ν'_{ij} and ν''_{ij} are the reactant and product chemical stoichiometric coefficients for ith species in jth reaction, and χ_i denotes the ith species. Here, $K_{f,j}$ and $K_{f,j}$ are the forward and backward

reaction rate constants, which are controlled by the Arrhenius law and chemical equilibrium condition:

$$K_{f,j} = A_j T^{\beta_j} \exp(-Ea_j/RT), \qquad K_{b,j} = K_{f,j}/K_{c,j} \tag{5}$$

where, A_j, β_j and Ea_j represent the pre-exponential factor, the temperature dependence exponent and the activation energy of reaction j. $K_{c,j}$ is the chemical equilibrium constant computed by:

$$K_{c,j} = \left(\frac{P_{atm}}{RT}\right)^{\sum_{j=1}^{N}(v''_{i,j}-v'_{i,j})} \cdot \exp\left(\frac{\Delta s_j^0}{R/W_i} - \frac{\Delta h_j^0}{RT/W_i}\right) \tag{6}$$

where, $P_{atm} = 101325$ Pa. s_i and h_i are standard entropy and standard enthalpy of formation for ith species. W_i is the molecular mass of the ith species. Here, the finite production rate of each chemical species $\overline{\omega}_i$ is obtained by combining the elementary chemical reactions in the chemical model such that:

$$\overline{\omega}_i = W_i \sum_{j=1}^{N_R}(v''_{i,j} - v'_{i,j}) \left\{\sum_{i=1}^{N} \alpha_{i,j}[X_i]\right\} \times \left\{K_{f,j}\prod_{i=1}^{N}[X_i]^{v'_{i,j}} - K_{b,j}\prod_{i=1}^{N}[X_i]^{v''_{i,j}}\right\} \tag{7}$$

where, $[X_i]$ is the mole concentration of ith species. $\alpha_{i,j}$ is the third body coefficient of the ith species in jth reaction.

Considering the stiffness of the source terms, Strang splitting scheme [60] is used to divide the governing equations into the flow equation and the chemical reaction equation [61], and solve these independent differential equations. The time step for these two sub-steps is half the time step of flow calculation:

$$U_t + [F(U)]_x + [G(U)]_y = 0 \tag{8}$$

$$U_t = S \tag{9}$$

where, Eq. (8) is the 2D Euler equation for multi-species flow without chemical reaction process. The third order TVD Runge-Kutta method [62] and the fifth order WENO-LF scheme [63] are employed to discretize the temporal term and convection term, respectively. The flow equation is decoupled:

$$\frac{\partial U}{\partial t} + A(U)\frac{\partial U}{\partial x} + B(U)\frac{\partial U}{\partial y} = 0 \tag{10}$$

where, $A(U)$ and $B(U)$ denote the Jacobian matrix in the x and y direction. The Roe average method is adopted to transform the governing equation (10) into a quasi-linear problem.

Eq. (9) is a purely chemical reaction equation. Especially, the chemical kinetic integration is evaluated by automatically generated optimized Fortran-77 functions in the line of Chemkin-III [64]. The stiff nature of the problem due to the chemical reaction calculation is solved by the DVODE package [65].

This study uses stoichiometric hydrogen-oxygen mixtures with highly diluted by 70% argon ($2H_2 + O_2 + 7Ar$) as the free inflow, because of this premixed mixture is relatively stable and the cellular detonation structure is regular. In recent years, the 9-species hydrogen-oxygen chemical mechanisms have been widely used in the studies of detonation characteristics. Among them, the structures of oblique detonation flow field captured by the 19-step mechanism of Jachimowski's paper [66] and the 34-step mechanism of Westbrook's paper [67] in the detonation simulation process are obviously different. And both of these mechanisms include key elementary reactions mentioned in reference [66] which are directly related to the combustion characteristic parameters. Therefore, based on the different characteristics of oblique detonation in these two chemical mechanisms, the formation and development processes of oblique detonation are studied in depth. The default inflow parameters are 1.0 atm and 298.15 K. The whole flow field has uniform density, velocity and pressure, which are calculated according to Mach number $Ma = 7.5$ and wedge angle $\theta = 30°$. Under this condition, the main field structure of oblique detonation is obviously different, which is convenient to study the characteristics of oblique detonation flow field.

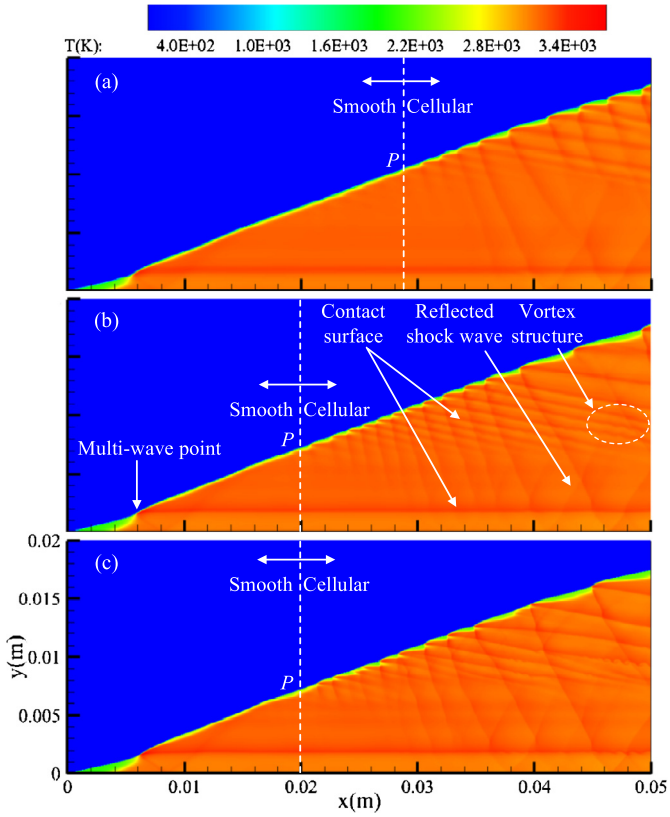

Fig. 2. Temperature with the grid sizes. (a) 70×60 μm^2. (b) 50×40 μm^2. (c) 30×20 μm^2.

3. Numerical results and discussion

3.1. Basic structure and resolution study

In order to capture the complete ODW structure and adjust the computational cost, resolution studies are performed. Fig. 2 shows the temperature for the case of $Ma = 7.5$ and $\theta = 30°$ under the 19-step chemical mechanism, displaying the results from the low-resolution to the high-resolution tests with the grid sizes of 70×60 μm^2, 50×40 μm^2 and 30×20 μm^2. It is clear that, with the increase of resolution, the multi-wave point moves just slightly downstream, and the reflected shock wave in the combustion product becomes more apparent. However, for 70×60 μm^2 grid size of Fig. 2(a), the initial instability position (P) on the oblique detonation wave surface moves downstream obviously, and the vortex structures generated by the interaction between the shock waves and the contact discontinuity surfaces cannot be revealed. By increasing the resolution, the features of the flow field with the grid size of 50×40 μm^2 are basically consistent with that of 30×20 μm^2 (such as: wave morphology and the cellular ODW surface instability, etc.).

For a more quantitative comparison, the pressure and temperature profiles along the line $y = 0.5$ mm under the 19-step chemical mechanism are plotted in Fig. 3. From upstream to downstream,

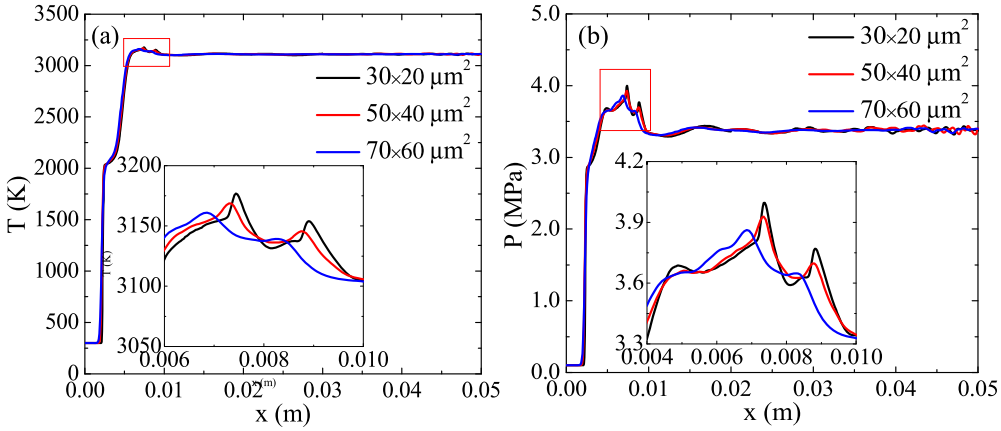

Fig. 3. Temperature (a) and pressure (b) along the line $y = 0.5$ mm with different grid sizes. (For interpretation of the colors in the figure(s), the reader is referred to the web version of this article.)

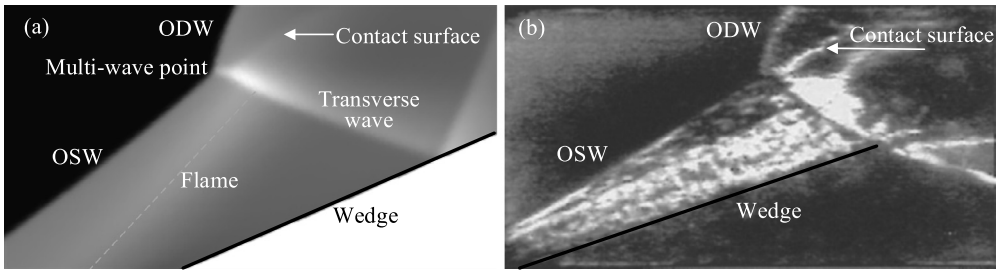

Fig. 4. (a) Density contour by numerical and (b) Schlieren image by experimental of the ODW flow field.

the temperature and pressure of the inflow mixture rise under the compression of the oblique shock wave. As the incoming mixture flows through the initiation field, the temperature and pressure fluctuate under the action of the wave system structures. The curves with different grid sizes are almost overlapped together except for the coarsest one with 70×60 μm^2. Moreover, there are almost 10 grids in the half reaction length of the completely premixed ODW field with grid size of 50×40 μm^2, which is deemed sufficient to capture the main physical and chemical processes. This resolution is sufficient for calculation of an overdriven ODW as that has been confirmed by Teng et al. [33]. In addition, the mesh convergence under the action of 34-step chemical mechanism also shows that the grid size 50×40 μm^2 can well describe the main features of the oblique detonation flow field. This is not described here, and the grid size 50×40 μm^2 is selected for the later simulations.

The basic structure of stationary oblique detonation has been confirmed by Viguier's experiments [25,43]. The experimental results of oblique detonation wave structure from Ref. [25] are selected to make a validation of the numerical method. One of their experiments, with the initial pressure $P_0 = 0.4$ bar, the initial temperature $T_0 = 293$ K, the inflow Mach number and wedge angle calculated according to the experimental condition are $Ma = 7.5$ and $\theta = 25°$, respectively. The density contour of the numerical result for the 19-step mechanism is shown in the Fig. 4 (a). It is clearly observed that the oblique detonation includes an oblique shock wave, an oblique detonation wave, a multi-wave point, a contact discontinuity surface and a transverse wave. Compared with the schlieren image of the flow field obtained from the experiment in Fig. 4 (b), it is shown that all the oblique detonation wave structures are similar. In addition, the flow field structure of oblique detonation obtained from the 34-step mechanism simulation result is also compared, and the main structure system is in good agreement with this experimental result, which will not be repeated it here. Therefore, the CFD method used in this paper can effectively simulate the complex wave structures in oblique detonation and meet the requirements of the numerical studies.

3.2. Formation and development of oblique detonation

Fig. 5 shows the flow field temperature and pressure for the case of $Ma = 7.5$, $\theta = 30°$ at different moments during the initiation stage of oblique detonation with the 19-step and 34-step chemical reaction models. The upper part is the temperature contour and the lower part is the pressure contour. It can be seen that the supersonic combustible inflow is compressed by wedge surface, producing a series of compression waves. An oblique shock wave is formed at the wedge tip, the temperature and pressure behind the shock increase accordingly. The combustion wave is formed from the wedge surface after the induction process, gradually converging on the front of the oblique shock wave. For the two chemical reaction models, the changes of the initial flow field under the interaction of compression wave and oblique shock wave are similar (2 μs). As the flow proceeds, the temperature and pressure increase but their distribution in flow field and the formation process of wave structures are obviously different. When $t = 4$ μs, the heat release of the chemical kinetic increases and a series of combustion waves are formed. As can be seen from the figure, the temperature, pressure and combustion wave angle α of the flow field under the 19-step mechanism are larger than those under the 34-step mechanism. For the 34-step mechanism, the position of the combustion wave is relatively lagging, and the coupling between the combustion wave front and the oblique shock wave front is relatively late. It shows that the acceleration of flame propagation is large and the heat release rate of chemical reaction is fast for 19-step mechanism.

To quantitatively analyze the characteristics of flow field in the initiation stage of oblique detonation under different chemical reaction models, the temperature and pressure of the flow field at the wedge surface on different moments in Fig. 5 are analyzed,

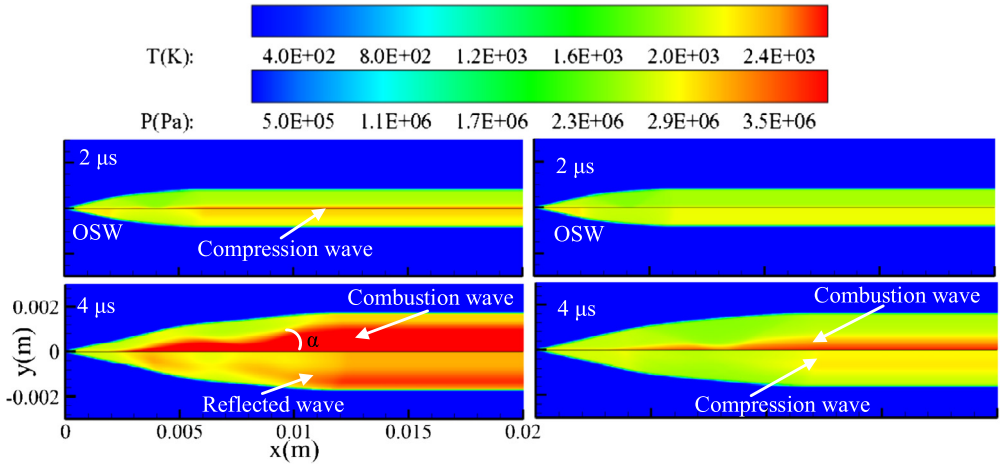

(a) 19-step chemical reaction model (b) 34-step chemical reaction model

Fig. 5. Temperature (upper) and pressure (lower) at different time during the initiation stage.

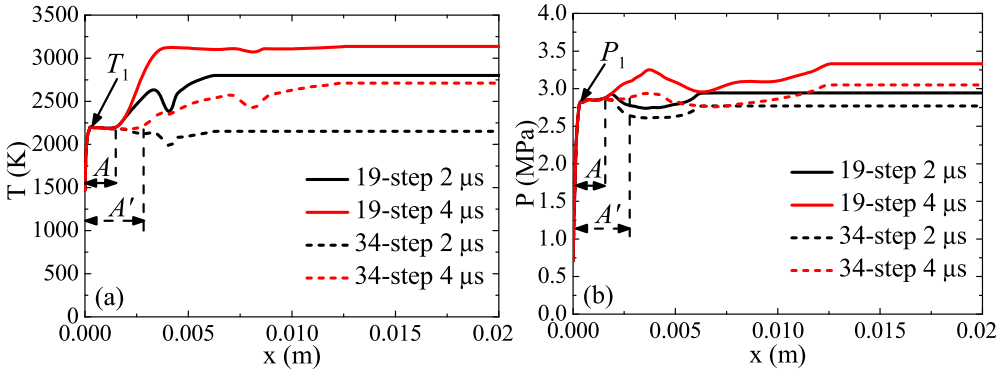

Fig. 6. Temperature (a) and pressure (b) along the wedge surface ($y = 0.0$ mm) at different time.

as shown in Fig. 6. In the initial stage, under the gas dynamics-controlling of compressibility, the changes of the flow field obtained by the simulation of different chemical reaction models are consistent, as mentioned above. The inflow flows through the oblique shock wave at $x = 0.0$ mm, and the temperature and pressure rise rapidly to $T_1 = 2206.4$ K and $P_1 = 2.87$ MPa (2 μs). Because the shock front in the flow field is curved, the flow direction behind the shock is inconsistent, resulting in a series of expansion waves. The temperature and pressure through the expansion waves along the x direction decrease first, and then increase under the action of the compression wave. As flow develops, the expansion waves move downstream with the curved position of the oblique shock wave front. Behind the induction region with constant temperature and pressure, as shown at 4 μs, the temperature of the flow field increases rapidly and the heat release process occurs. The combustion wave interacts with the compression wave behind the oblique shock, in the process of converging to the oblique shock wave. The induction region is formed between the combustion wave and the oblique shock wave at the wedge tip. For the 19-step mechanism, the length of induction region A is shorter than that of 34-step. With the same inflow conditions, the flow field is dominated by the aerodynamic process and transfers to the process controlled by the combined actions of aerodynamic and the chemical kinetic. Under the chemical kinetics-controlling behind the oblique shock wave, the exothermic rate is different for the two chemical mechanisms, resulting in different intensity of exothermic processes and induction region lengths.

As the reaction progresses, the combustion wave continues to propagate in the flow field. Fig. 7 is the contours of flow field at the development stage of oblique detonation. It can be seen that the combustion wave front and the oblique shock wave front are coupled to form oblique detonation wave. The density behind the non-reactive oblique shock wave and the oblique detonation wave are different, resulting in the contact discontinuity surface extending downstream. Under the influence of oblique detonation surface instability, new triple structures continue to form at the front (10 μs). The transverse waves pass through the contact discontinuity surfaces and intersect with the wedge surface, forming reflected shock waves (40 μs). The wave system structures in the flow field are quite different for two chemical reaction models. From Fig. 7 (a), under the interaction of transverse waves, reflected shock waves and contact discontinuity surfaces, the Kelvin-Helmholtz (K-H) vortex-rolling along the contact discontinuity surfaces (40 μs) appears in the downstream with the 19-step. For the oblique detonation flow field with the 34-step, as shown in Fig. 7 (b), in the flow field (40 μs), there are few triple structures on the front of the oblique detonation wave, and there are no multi-dimensional complex wave system structures. The structure of the oblique detonation flow field obtained by the 19-step chemical mechanism can be more refined, and the action of complex wave system can be clearly shown. The internal action mechanism of the oblique detonation flow field can be further studied.

In order to deeply analyze the propagation processes of shock front and combustion front during the formation and development of oblique detonation, the velocities of shock and flame are cal-

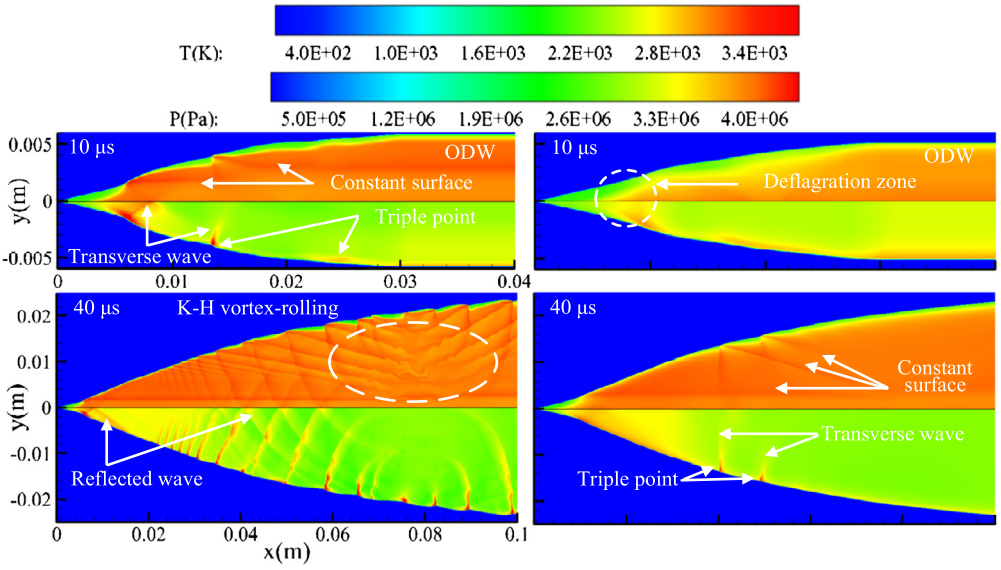

(a) 19-step chemical reaction model (b) 34-step chemical reaction model

Fig. 7. Temperature (upper) and pressure (lower) at different time during the development stage.

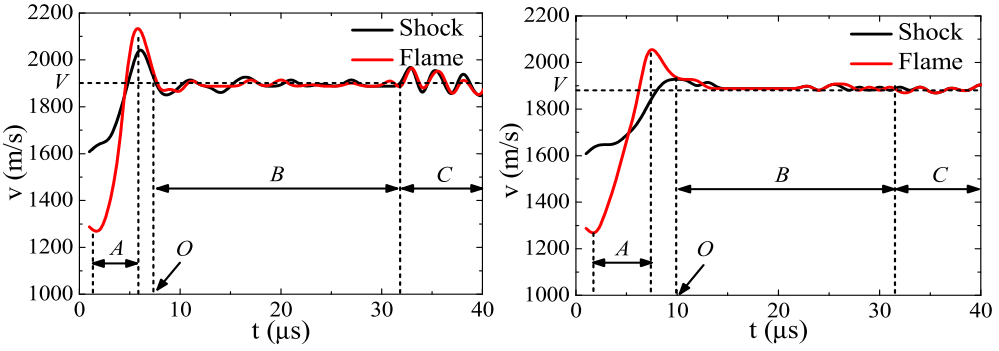

(a) 19-step chemical reaction model (b) 34-step chemical reaction model

Fig. 8. Propagation velocities of the leading shock wave front and the combustion wave front with time.

culated according to the propagation distance of shock wave front and combustion wave front along the normal direction of wave surface in a period of time. And, the maximum values of pressure gradient and temperature gradient in normal direction of wave surface near the outlet boundary are taken every 1 μs, to capture the positions of the leading shock wave front and the combustion wave front with time. Fig. 8 shows their propagation velocities with time under different chemical reaction models. It can be seen that the oblique detonation is formed after the flame acceleration stage *A*, and the velocity of the ODW front fluctuates during ODW development stage *B* and *C*. For different chemical reaction models, the processes of flame acceleration and detonation wave propagation are obviously different. According to period *A* in the Fig. 8, the 19-step mechanism has a larger slope of the flame front propagation velocity curve than 34-step mechanism, which means that the flame propagation acceleration is greater and the chemical reaction exothermic rate is faster under the action of 19-step mechanism. The oblique detonation wave is formed by the flame front coupled with the shock front at the moment *O*, which takes a very short time for 19-step. At this point, the propagation velocity of the combustion wave front is approximately equal to the velocity of the oblique shock wave front. At the early stage *B* of the oblique detonation wave development, the velocity of detonation wave front is relatively stable. While for the later stage *C*, the front velocity of oblique detonation wave appears periodic oscillation, which is caused by the continuous formation of triple structures on the detonation front propagating downstream. The number of triple structures on the detonation front under the action of 19-step mechanism is more than that of 34-step mechanism. Therefore, the oscillation of detonation wave front velocity is more violent and the frequency is higher for 19-step mechanism.

3.3. Oblique detonation wave characteristics

Fig. 9 shows the contours of the stationary oblique detonation flow field for different chemical reaction models. It can be seen from the figure that the oblique detonation wave front consists of two parts: the smooth oblique detonation wave near the upstream and the oblique detonation wave with multi-dimensional complex structure in the downstream. Compared with 34-step mechanism, under the 19-step chemical mechanism, the oblique detonation wave with the smooth section is short, and the wave system structures are clear. Besides, the K-H vortex-rolling structures and the cell structures appear in the downstream. The oblique detonation wave front tends to be linear in general, but bends locally. The structure around the mainstream multi-wave point is complex, and the wave system structures are different significantly for the two chemical reaction models. It is shown that the structure of oblique

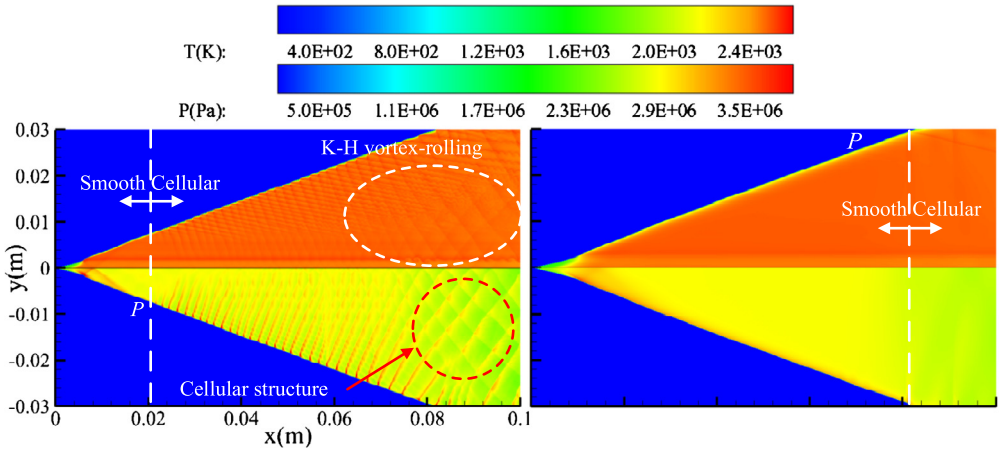

(a) 19-step chemical reaction model (b) 34-step chemical reaction model

Fig. 9. Temperature (upper) and pressure (lower) of the stationary oblique detonation.

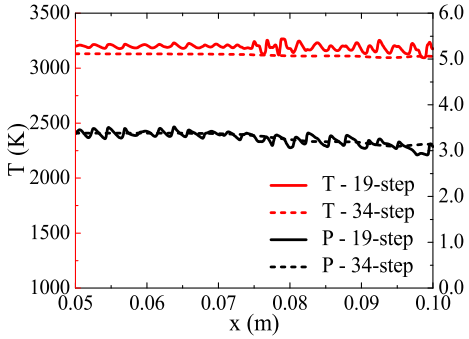

Fig. 10. Temperature and pressure of downstream along wedge surface ($y = 1.6$ mm).

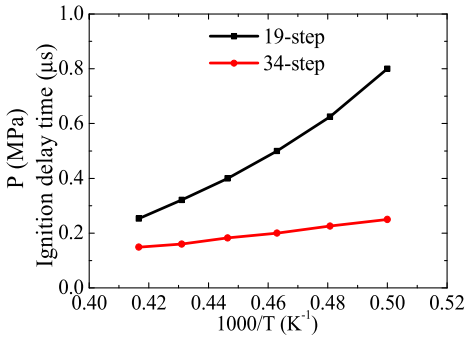

Fig. 11. Ignition delay time with temperature.

detonation front and the flow field structure behind detonation wave are obviously affected by the exothermic and combustion properties of different chemical reaction processes.

Fig. 10 shows the temperature and pressure of the downstream along wedge surface ($y = 1.6$ mm). The flow field parameters oscillate due to the existence of complex wave system structures for the 19-step mechanism, while the flow field of the 34-step mechanism is relatively uniform. Under different chemical reaction models, the pressure of the stationary oblique detonation downstream is approximately equal, but the temperature for the 19-step mechanism is a little higher than that of 34-step. Therefore, there are significant differences in the formation and consumption of intermediate components for two chemical reaction processes, and the heat release of the 19-step chemical reaction model is higher than that of 34-step.

According to the above analysis, the flow field structures are different under the action of two chemical reaction mechanisms. In order to reveal the internal mechanism, the ignition delay time is analyzed in depth. Fig. 11 shows the ignition delay time with temperature for different chemical reaction models. In this paper, the ignition delay time defines based on the rate of temperature increase. The time corresponding to maximum temperature gradient $(dT/dt)_{\max}$ in the variation of temperature with time is the ignition delay time. The figure shows that the ignition delay time at high temperature is approximately inversely proportional to the temperature, and the higher the temperature is, the shorter the ignition delay time is. The curves have different characteristics for two chemical models. Under the action of the 19-step mechanism, the ignition delay time curve has a larger slope, indicating that the corresponding auto-ignition process is more sensitive to the variation of temperature than that of 34-step. The temperature at different positions of the oblique detonation wave front is different, thus, the ignition delay time is different, resulting in different lengths of the induced region. Stress distribution is not uniform between induced regions with different thickness, resulting in uneven distribution of parameters such as pressure on the front. Under the action of force or parameters inhomogeneity, the triple wave structures are formed on the detonation wave front, and the oblique detonation flow flied becomes unstable. According to the above analysis, the ignition delay time of 19-step mechanism varies more greatly with a slight change of temperature at different positions of detonation wave front than that of 34-step mechanism, resulting in the auto-ignition process more unstable and more cellular.

Fig. 12 shows the flow field contours at the initiation region of the stationary oblique detonation formed by different chemical reaction models. For the 19-step mechanism, the detonation splits and forms the structure characterized by the λ-shaped shock at the end of the induction region, as shown in Fig. 12 (a). This structure is also shown in the letter [53]. It can be found out the transition from the oblique shock to the oblique detonation wave is achieved by one multi-wave point, which is abrupt transition associated with the divergent shock wave. The upstream branch of the divergent shock couples with the deflagration wave, and the other reflects in the combustion product. For 34-step mechanism, there is no transverse wave at the mainstream region. The oblique shock wave and the oblique detonation wave are connected by a curved shock wave. It's a smooth transition.

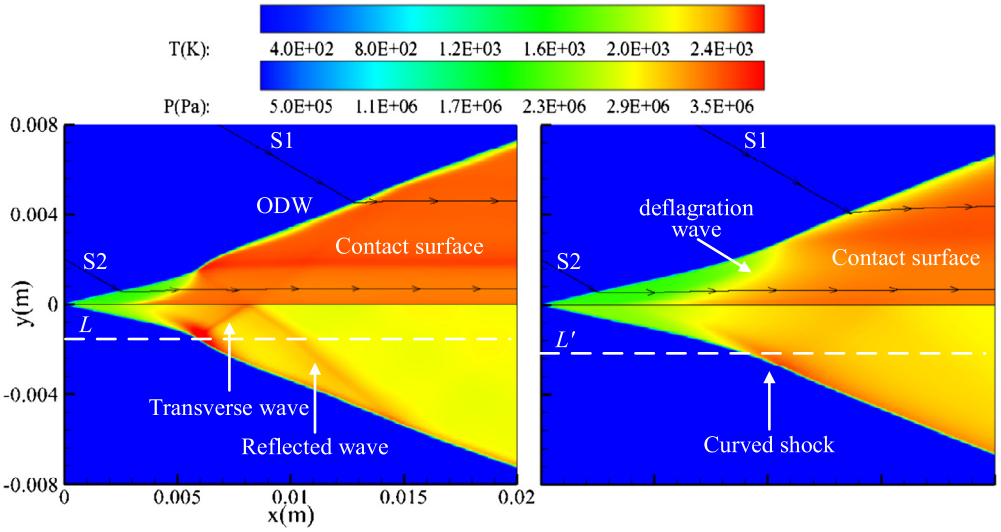

(a) 19-step chemical reaction model (b) 34-step chemical reaction model

Fig. 12. Temperature (upper) and pressure (lower) at the initiation region of the stationary oblique detonation.

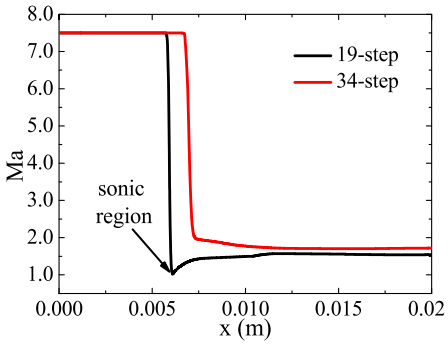

Fig. 13. Mach along the wedge surface near mainstream triple point.

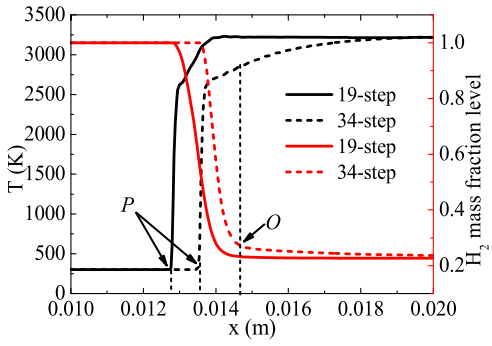

Fig. 14. Temperature and H_2 mass fraction level along streamline S1.

To further reveal the internal mechanism of different transition structures under the action of different reaction mechanisms, the local Mach number near transition region is analyzed. Fig. 13 shows the local Mach number along the wedge surface near the intersection of oblique shock wave and oblique detonation wave, see the line L or L' of Fig. 12. After the shock wave compression, the Mach number decreases. Under the 34-step mechanism, the whole flow field behind the oblique detonation wave is supersonic. While for the case of the 19-step mechanism, the minimum Mach number reaches about 1, forming a local sonic region. The appearance of this region is directly related to the formation of transverse wave in the transition region. From the following analysis of Fig. 14, it can be seen that the 19-step mechanism has a rapid temperature rise at the end of the induced region, resulting the pressure difference between the oblique post-detonation and the oblique post-shock at the transition region is greater than that of 34-step. To match the flow fields behind oblique detonation wave and oblique shock wave, a transverse wave is formed at their junction. Under the transverse wave compression, the Mach number decreases further forming a local sonic region at the transition zone. Besides, the appearance of the transverse wave in the mainstream field is the key factor for the formation of the multi-wave structure, which causes the abrupt transition from oblique shock wave to oblique detonation wave.

In order to further analyze the exothermic law of different chemical reaction models, we study their differences through the variations of temperature and H_2 component consumption on the flame front. Fig. 14 shows the variations of temperature and H_2 mass fraction level passing through the front of the oblique detonation wave along the streamline S1, which is extracted within the temperature contour of the fully formed ODW, as shown in Fig. 12. The mass fraction level is defined by the mass fraction of the component divided by its maximum value Y_i along the streamline. On the streamline S1, the most apparent feature is the almost complete coupling between the induction period and the exothermic period, because the constant value of temperature in induction region is hard to be observed (the point P corresponds to the oblique detonation front). It can be seen from the Fig. 14, the inflow mixture burns behind the oblique detonation wave, the temperature rises rapidly and the H_2 consumes quickly. Under the action of the 34-step chemical mechanism, the consumption rate of H_2 is relatively fast so the thickness of the flame zone is relatively thin. From the temperature variation behind the ODW (P), the temperature rises quickly and then stabilizes near the maximum value with a short time under the action of the 19-step mechanism. While for the 34-step, the temperature of the flow field continues to rise after H_2 is consumed in large quantities (at the point O) and takes more time to stabilization. The processes of combustion heat release are different under different chemical mechanisms, which are closely related to the formation process of intermediate radicals. The exothermic rate of the 19-step chemical mechanism is fast, which causes the temperature of the flow field rises quickly.

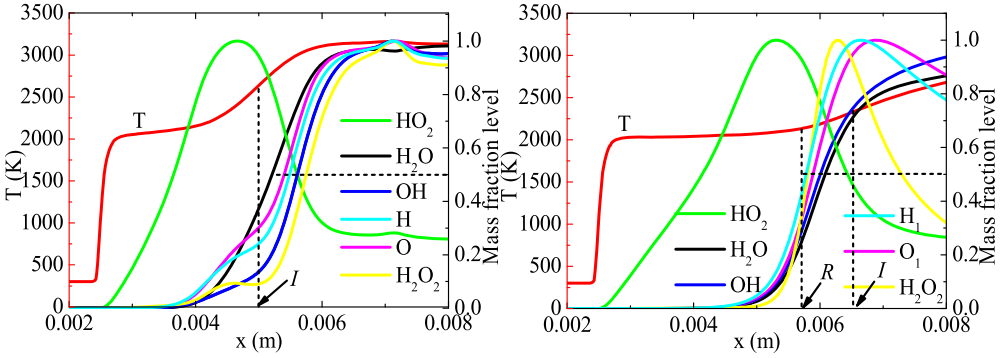

(a) 19-step chemical reaction model,

$$\max Y_{HO_2} = 4.831\times10^{-5},$$

$$\max Y_{H_2O} = 7.568\times10^{-2},\quad \max Y_{OH} = 1.664\times10^{-2},$$

$$\max Y_{H} = 8.205\times10^{-4},\quad \max Y_{O} = 5.667\times10^{-3},$$

$$\max Y_{H_2O_2} = 7.885\times10^{-7}.$$

(b) 34-step chemical reaction model,

$$\max Y_{HO_2} = 1.787\times10^{-5},$$

$$\max Y_{H_2O} = 6.595\times10^{-2},\quad \max Y_{OH} = 1.524\times10^{-2},$$

$$\max Y_{H} = 1.859\times10^{-3},\quad \max Y_{O} = 1.050\times10^{-2},$$

$$\max Y_{H_2O_2} = 1.298\times10^{-6}.$$

Fig. 15. Temperature and mass fraction levels along streamline S2 in the induction region.

3.4. Radicals formation and sensitivity analysis

In order to deeply understand the influence of chemical reaction processes on the formation and development of oblique detonation, the formation processes of radicals in the flow field are analyzed. Fig. 12 shows the extracted streamline S2 within the temperature contour of a fully formed ODW. Streamline S2 first passes through the shock-induced combustion region and then extends to the downstream of oblique detonation. Fig. 15 shows flow properties along streamline S2 in the induction region. It can be seen that the temperature remains constant after S2 passes through the oblique shock wave (at $x = 0.0025$ m). This shock causes the temperature and pressure to rise above the ignition point of the mixture. After the shock-induced combustion region, H_2O component and temperature increase rapidly, the heat starts to release along streamline S2. The position of I in the figure corresponds to the maximum value of temperature gradient, where is marked as the end of the induction region or the start of the exothermic region. The part from the oblique shock wave to the beginning of heat release is called the induction region. Along streamline S2, the HO_2 is the first to appear during the induction period, and goes rise to the formation of the other radicals and the combustion product. Therefore, the HO_2 radicals play a key role on the induction period for the two chemical reaction models. The HO_2 radicals serve for the chain-propagation step, and the massive existence of HO_2 provides the basic condition for the exothermic process. In the early stage of heat release, H, O, H_2O_2 etc. product and HO_2 consumes gradually. From Fig. 15, the formation process of H_2O_2 in the heat release period of the ODW flow field is different for two chemical reaction models. For 19-step mechanism, the sequence at the species reach 1% of their maximum values along streamline S2 is the following: H_2O_2, H, O, OH, H_2O. It can be seen that the H_2O_2 is of great significance for the occurrence of exothermic process. Because it appears first at the beginning of the exothermic heat, then other radicals and combustion product H_2O are generated, successively. During the early period of the exothermic process, the concentration of H_2O_2 is approximately constant and the total formation rates of H, O and OH radicals slow down, corresponding to temperature rising rapidly and heat releasing intensely. H_2O first reaches 50% of its maximum value along streamline S2, then the flow field is dominated by the generation process of combustion product H_2O. In the late stage of exothermic process, the concentration of H_2O_2 rises rapidly and the increase of temperature slows down. It indicates that the consumption of H_2O_2 is directly related to accelerate the exothermic rate of the chemical reaction. While for the 34-step mechanism, the sequence at each of the radicals 1% of their maximum values along streamline S2 is the following: H, O, OH, H_2O, H_2O_2. In the early stage of heat release, the H_2O_2 appears at the latest, but it reaches 50% of its maximum value first (at the position R of Fig. 15 (b)). Until now, the temperature of the flow field is approximately unchanged. Since then, the temperature of flow field increases gradually. The concentration of H_2O_2 reaches its maximum value and then starts to be consumed, which means the exothermic process is about to begin (at the position I). With the consumption of H_2O_2, the temperature of the flow field increases rapidly. The H_2O_2 is involved in major chain branching reactions that directly determines the exothermic rate of chemical kinetic and the parameters distribution on flame surface. From the above analyses, the H_2O_2 plays an important role on triggering and accelerating exothermic process, and then affects the wave morphology in the initiation region of the oblique detonation.

Fig. 16 shows the variations of radicals along the extracted streamline S2 which extends to the downstream of oblique detonation. The concentrations of radicals increase during the exothermic period of the chemical kinetic. As the streamline S2 passes through the combustion product flow field, under different chemical mechanisms, the radicals change obviously different, showing different properties. From the figure that under the action of 19-step mechanism, H, O, OH and H_2O_2 behave surprisingly more like combustion products than intermediate radicals. Because their concentrations do not decrease exponentially after reaching the maximum levels, but still remain near the maximum values. For the 19-step mechanism, the pressure at the locations of the transverse wave and the reflected wave of the transverse wave in the initiation region is high, leading to more radicals dissociate. The increase concentrations of radicals promote the chemical kinetic progress. The concentration of the main product H_2O goes up and the concentrations of the other radicals go down in these regions with high pressure. The high-pressure condition promotes the conversion of H, O, OH and H_2O_2 into the main product H_2O in 19-step mechanism. For the 34-step mechanism, as the exothermic process goes on, the concentrations of H, O, and H_2O_2 reach their peaks, and then consume in large quantities. The results show that H, O and H_2O_2 are intermediates in this chemical kinetic process. With the development of chemical reaction equilibrium, the concentrations of OH and H_2O reach their maximum values and remain at

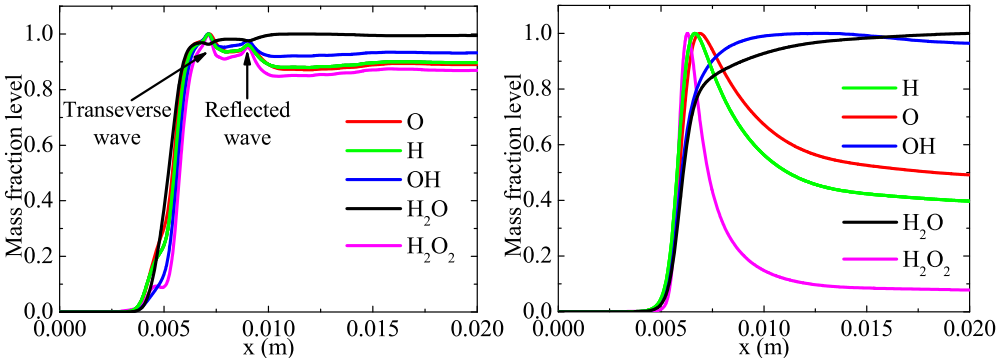

(a) 19-step chemical reaction model,

$\max Y_O = 5.667\times10^{-3}$, $\max Y_H = 8.205\times10^{-4}$, $\max Y_{OH} = 1.664\times10^{-2}$, $\max Y_{H_2O} = 7.710\times10^{-2}$, $\max Y_{H_2O_2} = 7.885\times10^{-7}$.

(b) 34-step chemical reaction model,

$\max Y_O = 1.050\times10^{-2}$, $\max Y_H = 1.859\times10^{-3}$, $\max Y_{OH} = 1.627\times10^{-2}$, $\max Y_{H_2O} = 7.605\times10^{-2}$, $\max Y_{H_2O_2} = 1.298\times10^{-6}$.

Fig. 16. O, H, OH and H_2O_2 mass fraction levels along streamline S2.

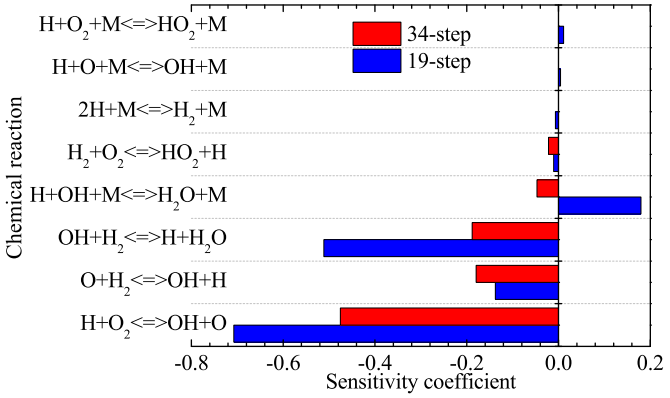

Fig. 17. Sensitivity analysis of H_2.

the high levels without being consumed exponentially for different chemical reaction models. The OH and H_2O are combustion products for the two chemical reaction models. In summary, H, O, and H_2O_2 have different properties in different chemical reaction models, resulting in slight differences in the quantities of heat release. Besides, the mass fraction of the product H_2O is relatively high under the action of 19-step, and the heat release is higher than that of 34-step.

During the heat release of the chemical reaction, the concentration of H_2 decreases rapidly. It is assumed that 90% of the maximum temperature is the end state of the exothermic process. In the case of $Ma = 7.5$, it is considered that the temperature of oblique detonation flow field at the late exothermic process is approximately 3200 K. In order to deeply understand the exothermic characteristics of oblique detonation flow field under different chemical reactions, the sensitivity of the reactant H_2 concentration to each reaction rate at about 3200 K is analyzed, see Fig. 17. There are eight chemical reactions which are sensitive to heat release, and the others with little effect on the exothermic process are not listed. The higher the value, the more obvious effect of the chemical reaction on heat release. The negative coefficient indicates that the reaction is more sensitive to H_2 consumption, while the positive coefficient indicates that it is more sensitive to H_2 production. It can be seen from the figure, the key reactions which have a great influence on the exothermic process are chain-branching reaction: $H + O_2 \Leftrightarrow OH + O$, $O + H_2 \Leftrightarrow OH + H$ and chain-propagation reaction: $OH + H_2 \Leftrightarrow H + H_2O$ for different chemical reaction models. The chain-branching reaction causes strong exothermic process, and the chain-propagation reaction creates conditions for the development of chain. Through sensitivity analysis of the two chemical models, it can be seen that the sensitivity coefficient of H_2 corresponding to each reaction is quite different in different chemical models, but the key reaction relative value in each chemical model is approximate. The process of chemical kinetics has global effect. In the process of H_2 consumption, the global effect of the H_2 sensitivity coefficient of the 19-step mechanism is significantly larger than that of the 34-step mechanism, indicating that the exothermic process of the 19-step mechanism is more intense. We can also see from Fig. 17 that $H + OH + M \Leftrightarrow H_2O + M$ has different sensitivity for H_2 in the rapid heat release period of different chemical models. For the 19-step mechanism, there is a large amount of H_2O in the rapid heat release region, as shown in Fig. 15, and the third-body component H_2O of this reaction has a high efficiency, which greatly promotes the reaction to go into the reverse direction. The production of large amounts of H radicals inhibits this chain-termination reaction and promotes the bonding of H radicals towards the production of H_2. While for 34-step mechanism, the concentration of H_2O is low. First, H radicals are consumed to produce H_2O, and the chain-termination reaction slows down the exothermic rate of the chemical kinetic. Then, the decrease of H radicals promotes the decomposition of H_2, therefore the sensitivity coefficient is negative. The reaction $H + O_2 \Leftrightarrow OH + O$ is the principal chain-branching reaction, and additional branching is provided by $O + H_2 \Leftrightarrow OH + H$. Together with the chain-termination reaction $H + OH + M \Leftrightarrow H_2O + M$, they play a major role on the exothermic process of chemical kinetic. From the above analysis, we can know that the exothermic rate of 19-step mechanism is faster than that of 34-step mechanism.

According to the results in Fig. 16, the radicals of H, O and H_2O_2 have different properties in different chemical reaction models. Next, the sensitivity of the H and H_2O_2 concentrations to the key reactions at the late stage of exothermic process is studied, see Fig. 18. It can be seen from the figure, the reaction $H + OH + M \Leftrightarrow H_2O + M$ is sensitive to the consumption of H and H_2O_2 for the two chemical mechanisms, and the absolute value of the sensitivity coefficient of 34-step is larger. It indicates that the reaction $H + OH + M \Leftrightarrow H_2O + M$ of the 34-step mechanism promotes the consumption of H and H_2O_2 more obviously. The radicals H are consumed to product stable H_2O, and this chemical reaction goes towards the positive direction, resulting in chain-termination reaction. However, H and H_2O_2 have completely different sensitiv-

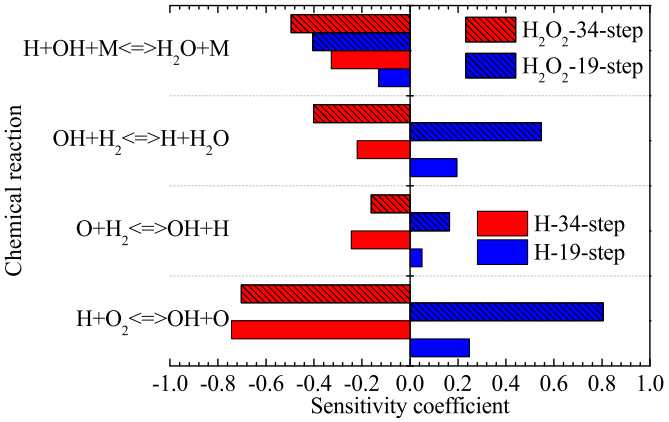

Fig. 18. Sensitivity analysis of H_2O_2 and H.

ity to chain-branching reaction and chain-propagation reaction on the two chemical mechanisms. For the 19-step chemical reaction mechanism, the H and H_2O_2 exist as the form of products from the results of Fig. 16. And, the key chemical reaction channels of the exothermic process are sensitive to the production of H and H_2O_2 from Fig. 18, so the concentrations of H and H_2O_2 do not decrease exponentially. However, the key channels of exothermic process in the 34-step mechanism have a sensitivity on the consumption of H and H_2O_2. The overall trends of the concentrations of H and H_2O_2 in this chemical mechanism are decrease. They behave as the intermediate radicals in the exothermic process. The concentrations of H and H_2O_2 have different change rules, showing different properties in the exothermic process of different chemical reaction models. And that, the consumption of H_2O_2 has an effect on accelerating the heat release of chemical reaction, resulting in the difference exothermic rates for the 19-step and 34-step mechanism. In addition, different compositions of products result in different heat release in the flow field.

4. Summary and conclusions

To explore the effect of different chemical reaction models on the fundamental characteristics of ODW, we compare the formation and development of ODW under two detailed chemistry models which are 19-step reactions with 9 species mechanism and 34-step reactions with 9 species mechanism. The main conclusions are drawn as follows:

(1) The initiation process of oblique detonation is affected by the propagation velocity of combustion wave. The higher the exothermic rate of chemical reaction, the faster the formation of oblique detonation. The 19-step mechanism is suitable for studying the interaction process between wave system and the formation mechanism of the instability structure in the oblique detonation flow field. The 34-step mechanism is suitable for studying the characteristics of oblique detonation, such as structure parameters and propagation properties of ODW, pressurization and exothermic characteristics of oblique detonation flow field.

(2) The flow field structure of oblique detonation is mainly determined by the chemical kinetic parameters. For the 19-step mechanism, the ignition delay time is sensitive to the change of temperature, and the exothermic rate of chemical reaction process is fast. Compared with the simulation results of 34-step mechanism, the wave morphology of oblique detonation is more complex, and the transverse wave is more likely to form in the initiation region. The mainstream transverse wave plays an important role on the formation of a sonic region, which is directly related to the abrupt transition structure of OSW-ODW.

(3) The study on the formation of radicals in the induced region of ODW shows that HO_2 is the first radical to appear in the induced region, which plays a key role on the induction period of oblique detonation. The exothermic process of chemical reaction is directly related to the formation of radicals, and H_2O_2 plays an important role on triggering and accelerating the exothermic process. During the exothermic period, the properties of H, O and H_2O_2 are similar to the product H_2O in the 19-step chemical mechanism. While, for the 34-step chemical mechanism, H, O and H_2O_2 exist as intermediate forms.

Declaration of competing interest

We declare that we have no conflict of interest.

Acknowledgements

The authors would like to acknowledge the National Natural Science Foundation of China (Grant No. 52071103) for supporting this work.

References

[1] G.D. Roy, S.M. Frolov, A.A. Borisov, D.W. Netzer, Pulse detonation propulsion: challenges, current status, and future perspective, Prog. Energy Combust. 30 (2004) 545–672.
[2] J. Chambers, K. Ahmed, Turbulent flame augmentation using a fluidic jet for Deflagration-to-Detonation, Fuel 199 (2017) 616–626.
[3] Y. Liu, W. Zhou, Y. Yang, Z. Liu, J. Wang, Numerical study on the instabilities in H_2-air rotating detonation engines, Phys. Fluids 30 (2018) 046106.
[4] X. Cai, J. Liang, R. Deiterding, Y. Mahmoudi, M. Sun, Experimental and numerical investigations on propagating modes of detonations: detonation wave/boundary layer interaction, Combust. Flame 190 (2018) 201–215.
[5] Z. Zhang, K. Ma, W. Zhang, X. Han, Y. Liu, Z. Jiang, Numerical investigation of a Mach 9 oblique detonation engine with fuel pre-injection, Aerosp. Sci. Technol. 105 (2020) 106054.
[6] J. Urzay, Supersonic combustion in air-breathing propulsion systems for hypersonic flight, Annu. Rev. Fluid Mech. 50 (2017) 593–627.
[7] Y. Fang, Z. Hu, H. Teng, Numerical investigation of oblique detonations induced by a finite wedge in a stoichiometric hydrogen-air mixture, Fuel 234 (2018) 502–507.
[8] M. Valorani, M.D. Giacinto, C. Buongiorno, Performance prediction for oblique detonation wave engines (ODWE), Acta Astronaut. 48 (2001) 211–228.
[9] P. Wolanski, Detonative propulsion, Proc. Combust. Inst. 34 (2013) 125–158.
[10] K. Kailasanath, Review of propulsion applications of detonation waves, AIAA J. 38 (2015) 1698–1708.
[11] J. Verreault, A.J. Higgins, Initiation of detonation by conical projectiles, Proc. Combust. Inst. 33 (2011) 2311–2318.
[12] Y. Fang, Z. Zhang, Z. Hu, X. Deng, Initiation of oblique detonation waves induced by a blunt wedge in stoichiometric hydrogen-air mixtures, Aerosp. Sci. Technol. 92 (2019) 676–684.
[13] H. Teng, H.D. Ng, Z. Jiang, Initiation characteristics of wedge-induced oblique detonation waves in a stoichiometric hydrogen-air mixture, Proc. Combust. Inst. 36 (2017) 2735–2742.
[14] G. Li, G. Zhang, Y. Zhang, L. Ji, S. Gao, Influence of viscous boundary layer on initiation zone structure of two-dimensional oblique detonation wave, Aerosp. Sci. Technol. 104 (2020) 106019.
[15] M.J. Kaneshige, J.E. Shepherd, Oblique detonation stabilized on a hypervelocity projectile, Symp., Int., Combust. 26 (1996) 3015–3022.
[16] J. Kasahara, T. Arai, S. Chiba, K. Takazawa, Y. Tanahashi, A. Matsuo, Criticality for stabilized oblique detonation waves around spherical bodies in acetylene/oxygen/krypton mixtures, Proc. Combust. Inst. 29 (2002) 2817–2824.
[17] H. Teng, W. Zhao, Z. Jiang, A novel oblique detonation structure and its stability, Chin. Phys. Lett. 24 (2007) 1985–1988.
[18] S. Maeda, J. Kasahara, A. Matsuo, Oblique detonation wave stability around a spherical projectile by a high time resolution optical observation, Combust. Flame 159 (2012) 887–896.
[19] Z. Ren, B. Wang, Numerical study on stabilization of wedge-induced oblique detonation waves in premixing kerosene-air mixtures, Aerosp. Sci. Technol. 107 (2020) 106245.
[20] R.A. Gross, Oblique detonation waves, AIAA J. 1 (1963) 1225–1227.
[21] D.T. Pratt, J.W. Humphrey, D.E. Glenn, Morphology of standing oblique detonation waves, J. Propuls. Power 7 (1991) 837–845.
[22] C. Li, K. Kailasanath, E.S. Oran, Detonation structures behind oblique shocks, Phys. Fluids 6 (1994) 1600–1611.

[23] L. Yang, L. Yue, Q. Zhang, X. Zhang, Numerical study on the shock/combustion interaction of oblique detonation waves, Aerosp. Sci. Technol. 104 (2020) 105938.
[24] J.H.S. Lee, The Detonation Phenomenon, Cambridge University Press, New York, 2008.
[25] C. Viguier, L.F.F. da Silva, D. Desbordes, B. Deshaies, Onset of oblique detonation waves: comparison between experimental and numerical results for hydrogen-air mixtures, Symp., Int., Combust. 26 (1996) 3023–3031.
[26] M.V. Papalexandris, A numerical study of wedge-induced detonations, Combust. Flame 120 (2000) 526–538.
[27] G. Xiang, X. Li, X. Sun, X. Chen, Investigations on oblique detonations induced by a finite wedge in high altitude, Aerosp. Sci. Technol. 95 (2019) 105451.
[28] H. Teng, Z. Jiang, On the transition pattern of the oblique detonation structure, J. Fluid Mech. 713 (2012) 659–669.
[29] Y. Liu, Y.S. Liu, D. Wu, J. Wang, Structure of an oblique detonation wave induced by a wedge, Shock Waves 26 (2016) 161–168.
[30] K. Iwata, S. Nakaya, M. Tsue, Wedge-stabilized oblique detonation in an inhomogeneous hydrogen-air mixture, Proc. Combust. Inst. 36 (2017) 2761–2769.
[31] Y. Zhang, P. Yang, H. Teng, H.D. Ng, C. Wen, Transition between different initiation structures of wedge-induced oblique detonations, AIAA J. 56 (2018) 4016–4023.
[32] J.Y. Choi, E.J.R. Shin, I.S. Jeung, Unstable combustion induced by oblique shock waves at the non-attaching condition of the oblique detonation wave, Proc. Combust. Inst. 32 (2009) 2387–2396.
[33] H. Teng, Z. Jiang, H.D. Ng, Numerical study on unstable surfaces of oblique detonations, J. Fluid Mech. 744 (2014) 111–128.
[34] Y. Liu, D. Wu, S. Yao, J. Wang, Analytical and numerical investigations of wedge-induced oblique detonation waves at low inflow Mach number, Combust. Sci. Technol. 187 (2015) 843–856.
[35] P. Yang, H. Teng, Z. Jiang, H.D. Ng, Effects of inflow Mach number on oblique detonation initiation with a two-step induction-reaction kinetic model, Combust. Flame 193 (2018) 246–256.
[36] J.Y. Choi, D.W. Kim, I.S. Jeung, F. Ma, V. Yang, Cell-like structure of unstable oblique detonation wave from high-resolution numerical simulation, Proc. Combust. Inst. 31 (2007) 2473–2480.
[37] J. Verreault, A.J. Higgins, R.A. Stowe, Formation of transverse waves in oblique detonations, Proc. Combust. Inst. 34 (2013) 1913–1920.
[38] P. Yang, H.D. Ng, H. Teng, Z. Jiang, Initiation structure of oblique detonation waves behind conical shocks, Phys. Fluids 29 (2017) 086104.
[39] H.D. Ng, Effects of activation energy on the instability of oblique detonation surfaces with a one-step chemistry model, Phys. Fluids 30 (2018) 106110.
[40] H. Teng, H.D. Ng, K. Li, C. Luo, Z. Jiang, Evolution of cellular structures on oblique detonation surfaces, Combust. Flame 162 (2015) 470–477.
[41] Y. Zhang, J. Gong, T. Wang, Numerical study on initiation of oblique detonations in hydrogen-air mixtures with various equivalence ratios, Aerosp. Sci. Technol. 49 (2016) 130–134.
[42] P. Yang, H. Teng, H.D. Ng, Z. Jiang, A numerical study on the instability of oblique detonation waves with a two-step induction-reaction kinetic model, Proc. Combust. Inst. 37 (2019) 3537–3544.
[43] C. Viguier, A. Gourara, D. Desbordes, Three-dimensional structure of stabilization of oblique detonation wave in hypersonic flow, Symp., Int., Combust. 27 (1998) 2207–2214.
[44] Z. Hu, Z. Jiang, Wave dynamic processes in cellular detonation reflection from wedges, Acta Mech. Sin. 23 (2007) 33–41.
[45] H.D. Ng, M.I. Radulescu, A.J. Higgins, N. Nikiforakis, J.H.S. Lee, Numerical investigation of the instability for one-dimensional Chapman-Jouguet detonations with chain-branching kinetics, Combust. Theory Model. 9 (2005) 385–401.
[46] M.I. Radulescu, G.J. Sharpe, D. Bradley, A universal parameter quantifying explosion hazards, detonability and hot spot formation: the χ number, in: Proceedings of the Seventh International Seminar Fire and Explosion Hazards, 2013.
[47] J. Tang, M.I. Radulescu, Dynamics of shock induced ignition in Fickett's model: influence of χ, Proc. Combust. Inst. 34 (2013) 2035–2041.
[48] C. Yan, H. Teng, X. Mi, H.D. Ng, The effect of chemical reactivity on the formation of gaseous oblique detonation waves, Aerospace 6 (2019) 62.
[49] N.N. Smirnov, V.F. Nikitin, L.I. Stamov, D.I. Altoukhov, Supercomputing simulations of detonation of hydrogen-air mixtures, Int. J. Hydrog. Energy 40 (2015) 11059–11074.
[50] B. Zhang, The influence of wall roughness on detonation limits in hydrogen-oxygen mixture, Combust. Flame 169 (2016) 333–339.
[51] B. Zhang, L. Pang, X. Shen, Y. Gao, Measurement and prediction of detonation cell size in binary fuel blends of methane/hydrogen mixtures, Fuel 172 (2016) 196–199.
[52] H. Wei, Y. Shang, J. Cai, M. Pan, G. Shu, R. Chen, Numerical study on transition of hydrogen/air flame triggered by auto-ignition under effect of pressure wave in an enclosed space, Int. J. Hydrog. Energy 42 (2017) 16877–16886.
[53] H. Teng, Y. Zhang, Z. Jiang, Numerical investigation on the induction zone structure of the oblique detonation waves, Comput. Fluids 95 (2014) 127–131.
[54] Y. Fang, Z. Hu, H. Teng, Z. Jiang, H.D. Ng, Numerical study of inflow equivalence ratio inhomogeneity on oblique detonation formation in hydrogen-air mixtures, Aerosp. Sci. Technol. 71 (2017) 256–263.
[55] G. Fusina, J.P. Sislian, B. Parent, Formation and stability of near Chapman-Jouguet standing oblique detonation waves, AIAA J. 43 (2005) 1591–1604.
[56] B. Zhang, H. Liu, Y. Li, The effect of instability of detonation on the propagation modes near the limits in typical combustible mixtures, Fuel 253 (2019) 305–310.
[57] D. Sziroczak, H. Smith, A review of design issues specific to hypersonic flight vehicles, Prog. Aerosp. Sci. 84 (2016) 1–28.
[58] C. Li, K. Kailasanath, E.S. Oran, Effects of boundary layers on oblique-detonation structures, in: Aerospace Sciences Meeting, vol. 450, 2013.
[59] M.W. Chase, JANAF thermochemical tables, 3rd ed., Parts I and II, J. Phys. Chem. Ref. Data 14 (1985).
[60] W.G. Strang, On the construction and comparison of difference schemes, SIAM J. Numer. Anal. 5 (1968) 506–517.
[61] X. Hu, B.C. Khoo, D. Zhang, Z. Jiang, The cellular structure of a two-dimensional $H_2/O_2/Ar$ detonation wave, Combust. Theory Model. 8 (2004) 339–359.
[62] C. Shu, S. Osher, Efficient implementation of essentially non-oscillatory shock-capturing schemes, J. Comput. Phys. 77 (1988) 439–471.
[63] G. Jiang, C. Shu, Efficient implementation of weighted ENO schemes, J. Comput. Phys. 126 (1996) 202–228.
[64] R.J. Kee, F.M. Rupley, E. Meeks, J.A. Miller, CHEMKIN-III: A FORTRAN Chemical Kinetics Package for the Analysis of Gas-Phase Chemical and Plasma Kinetics, Sandia National Labs., Livermore, CA (United States), 1996.
[65] P.N. Brown, G.D. Byrne, A.C. Hindmarsh, VODE: a variable-coefficient ODE solver, SIAM J. Sci. Stat. Comput. 10 (1989) 1038–1051.
[66] C.J. Jachimowski, An analytical study of the hydrogen-air reaction mechanism with application to scramjet combustion, NASA Technical Paper 2791, 1988.
[67] C.K. Westbrook, Chemical kinetics of hydrocarbon oxidation in gaseous detonations, Combust. Flame 46 (1982) 191–210.